Environmental Science Nano

ROYAL SOCIETY OF CHEMISTRY

PAPER

View Article Online
View Journal

Cite this: DOI: 10.1039/d2en00361a

Optimizing the synergistic effect of $CuWO_4$/CuS hybrid composites for photocatalytic inactivation of pathogenic bacteria†

Xiuli Dong ,‡§[a] Rowan R. Katzbaer, ‡[b] Basant Chitara,[a] Li Han, [c] Liju Yang, [d] Raymond E. Schaak *[b] and Fei Yan *[a]

Herein, we report an effective strategy to maximize the antimicrobial activity of $CuWO_4$/CuS hybrid composites, prepared by simply mixing $CuWO_4$ and CuS nanopowders with varying weight ratios in phosphate buffered saline solution by ultrasound. The tested bacteria included Gram negative (G^-) pathogenic bacteria *Salmonella typhi*, Gram positive (G^+) pathogenic bacteria *Staphylococcus aureus*, and G^+ bacteria *Bacillus subtilis*. The as-prepared composites exhibited much enhanced antibacterial efficiency compared with individual $CuWO_4$ and CuS nanopowders under white light irradiation. The checkerboard array analysis revealed that the combination of 8 μg mL^{-1} $CuWO_4$ and 2 μg mL^{-1} CuS was the most efficient and generated the optimal synergistic effect, showing a complete killing effect on all the tested bacteria from 3 strains with ~5.8 log cell reduction. The significantly enhanced catalytic efficiency can be ascribed to the formation of a type-II heterojunction between $CuWO_4$ and CuS, which can effectively improve the charge separation efficiency and increase the light absorption. Moreover, the hybrid composites prepared by ultrasound-assisted physical mixing can effectively increase the interface area, which greatly facilitates the charge mobility and transfer in the interfaces between $CuWO_4$ and CuS. This study offers new insights into the integration of different semiconductors to optimize their synergistic effect on antimicrobial activities for water disinfection.

Received 12th April 2022,
Accepted 2nd October 2022

DOI: 10.1039/d2en00361a

rsc.li/es-nano

Environmental significance

Microbial contamination poses a serious risk in water resources worldwide. Despite considerable progress on the development of hybrid photocatalytic semiconductors for wastewater treatment and disinfection applications, very little is currently known about how to optimize the synergistic effect between two different semiconductor photocatalysts. In this study, for the first time, the broth microdilution checkerboard assay was adapted to systematically evaluate the antibacterial efficacy of nanopowders of $CuWO_4$ and CuS individually in comparison with hybrid composites prepared by mixing $CuWO_4$ and CuS with varying weight ratios. This method provided a way to find the best and most effective combination of antimicrobial photocatalysts. These findings have significant implications for controlled coupling of two or more semiconductors with suitable bandgaps to develop new and effective antimicrobial materials for water disinfection.

1. Introduction

Pathogens are the leading cause of many infectious diseases and developing antibacterial materials is a priority for global health. There are an estimated 31 major pathogens acquired in the United States each year, causing 9.4 million episodes of foodborne illness, about 55 000 hospitalizations, and over 1000 deaths.[1] In these outbreaks, *Staphylococcus aureus* (*S. aureus*) caused 3% of foodborne illnesses, and *Salmonella* spp. caused 28% of deaths.[1,2] The treatment of bacterial infections can be difficult when an antibiotic resistant function was developed in these bacteria. It has been reported that mutant antibiotic resistant strains such as

[a] *Department of Chemistry and Biochemistry, North Carolina Central University, Durham, NC 27707, USA. E-mail: fyan@nccu.edu, xdong@campbell.edu*
[b] *Department of Chemistry, The Pennsylvania State University, University Park, PA 16802, USA. E-mail: res20@psu.edu*
[c] *RTI International, Research Triangle Park, NC 27709, USA*
[d] *Department of Pharmaceutical Sciences, North Carolina Central University, Durham, NC 27707, USA*

† Electronic supplementary information (ESI) available. See DOI: https://doi.org/10.1039/d2en00361a

‡ Equal contribution.

§ Current address: School of Osteopathic Medicine, Campbell University, Lillington, NC 27506.

methicillin resistant *S. aureus* (MRSA) have been transmitted rapidly through hospital facilities and personal care products, leading to an uncontrollable problem.[3] Moreover, some environmental pathogens, such as *Bacillus anthracis* (*B. anthracis*), have been used as biological weapons by terrorists. *B. anthracis*, the etiologic agent of anthrax, is a Gram positive spore-forming bacterium.[4] *B. anthracis* spores could enter the human or animal's body through skin lesions, lungs, or the gastrointestinal route and cause severe illness.[4]

Many traditional antimicrobial reagents have been used to inactivate pathogenic bacteria. However, these chemicals are often toxic, creating potentially major issues in environmental and ecological systems and raising public health concerns.[5] As one of the new promising antimicrobial strategies, photocatalysis has emerged as an effective green solution for disinfection applications. The antimicrobial effect of photocatalysts was first found in titanium dioxide (TiO_2) by Matsunaga *et al.* in 1985.[8] Unfortunately, TiO_2 only absorbs UV light which accounts for a small fraction (~4%) of the entire solar spectrum.[9] Some photocatalysts, such as graphitic carbon nitride (g-C_3N_4)[6] and hybrid graphene oxide–silver nanoparticle composites,[7] have been reported to be able to inactivate antibiotic-resistant bacteria under visible light irradiation.[6] Thus, it is of great interest to develop photocatalysts that can yield high reactivity under visible light so that a great portion (~45%) of the solar spectrum is utilized in photocatalytic destruction of bacteria.[9]

Copper tungstate ($CuWO_4$) is an efficient visible light responsive photocatalyst with unique properties, including eco-friendliness, low cost, optimum band edge potential, and remarkable stability under oxidative and acidic conditions.[10] Benko *et al.*[11] first reported the photoelectrochemical properties of $CuWO_4$ in 1982. Since then, many efforts have been made to improve its photocatalytic and photoelectrochemical performance. One such strategy to improve the photocatalytic performance of $CuWO_4$ is to create a composite material with a photocathode, as $CuWO_4$ has the appropriate conduction band energy to act as a photoanode for the oxygen evolution half-reaction of water.[12,13] Its conduction band edge potential is more positive than that of CuO.[14]

Several studies have reported that $CuWO_4$ shows antimicrobial effects. For instance, it was reported that $CuWO_4$ demonstrated strong antimicrobial activity against *Candida albicans* and *S. aureus* by the disk diffusion assay.[15] Gupta *et al.*[16] synthesized the Z-scheme composite g-C_3N_4/$CuWO_4$, which showed the photocatalytic degradation of *S. aureus* and *E. coli* bacteria with 0.9 and 1.15 log reduction, respectively. Vignesh *et al.*[17] synthesized CdS and $CuWO_4$ modified TiO_2 nanoparticles, displaying a strong inactivation effect on *P. aeruginosa*.

Copper sulphide (CuS) is another visible-light-driven photocatalyst. Nonporous CuS exhibits excellent photocatalytic activity on the degradation of methylene blue (MB), methyl orange (MO), and rhodamine B (RhB).[18] CuS also shows excellent antimicrobial activity against bacteria such as *S. aureus* and *E. coli*.[19] Antimicrobial effects were also observed for CuS nanocrystals modified with different moieties, including Au,[20] lysozyme,[21] L-alanine and L-aspartic acid,[22] *etc.* It was reported that Au@CuS core–shell nanoparticles were highly effective in inhibiting the growth of *B. anthracis* vegetative cells.[20]

To enhance the performance of photocatalysts, the most common strategy is to form a heterojunction structure with other semiconductors. The generation of new heterojunctions by semiconductors with different bandgap energies and band edge potentials is beneficial for the separation and stabilization of photogenerated electrons and holes, can adjust the absorption range of light to lower energy, and facilitate the photocatalysis process.[23–26] However, it is a significant challenge to optimize the composition of these semiconductors to achieve maximum efficiency. In the area of medical science, a broth microdilution checkerboard method has been used to evaluate the antimicrobial synergistic effect of the combination of two drugs *in vitro*.[27] In the checkerboard assay, two antimicrobial drugs are tested in 2-fold serial dilutions with all possible combinations in 96-well plates. The results can be used to determine the interaction of the two drugs and provide the optimal combinations. It might be feasible to use this method with some modifications to optimize the antimicrobial synergistic effect of a hybrid composite that consists of two different semiconductor photocatalysts with varying weight ratios.

In this work, $CuWO_4$ was synthesized *via* a solid-state reaction. The antimicrobial activity of hybrid composites, which were prepared by mixing $CuWO_4$ and CuS with varying weight ratios in PBS buffer solution by ultrasound, was examined under the irradiation of white light (60 W). The tested bacteria included Gram negative (G^-) bacteria *Salmonella typhi* (*S. typhi*), Gram positive (G^+) bacteria *S. aureus*, and G^+ bacteria *Bacillus subtilis* (*B. subtilis*) which were used as a surrogate of pathogenic *B. anthracis*. To the best of our knowledge, there is only one other report on the fabrication of $CuWO_4$/CuS hybrid composites by physical mixing, used for photodegradation of RhB.[28] It is anticipated that the as-prepared composite will be able to broaden the light response range, prolong the life of photogenerated electrons and holes, and enhance the photocatalytic activity of $CuWO_4$. This approach is poised to find optimal semiconductor combinations for pathogen disinfection. This is the first instance that the modified broth microdilution checkerboard assay was used to optimize the synergistic effect of two different semiconductors for antimicrobial activity.

2. Materials and methods

2.1 Chemicals

CuS (99.8% purity) and WO_3 (99.8% purity) were purchased from Alfa Aesar. CuO (>99% purity) and isopropanol were purchased from Sigma Aldrich (St. Louis, MO). *S. typhi*, *S.*

aureus, and *B. subtilis* were purchased from the American Type Culture Collection (ATCC; Manassas, VA).

2.2 Synthesis of $CuWO_4$

The bulk $CuWO_4$ powder was synthesized from stoichiometric amounts of CuO and WO_3. The powders were ground together, placed in an alumna crucible, and fired in air at 800 °C for 24 hours.

2.3 Characterization

2.3.1 Powder X-ray diffraction. The powder X-ray diffraction (PXRD) scans were performed on a Malvern Panalytical XPert Pro MPD instrument with a copper source, using line focus and reflection mode. Simulated patterns were calculated from data retrieved from Springer Materials.

2.3.2 Scanning electron microscopy/energy-dispersive X-ray spectroscopy. $CuWO_4$ and CuS powders were suspended in water by probe sonication (Qsonica, XL-2000 series, output wattage at 6) for 10 minutes. The prepared suspensions were drop cast onto SEM silicon wafer and allowed to dry for imaging. Scanning electron microscopy (SEM) images were collected with an FEI Quanta 200 Environmental scanning electron microscope. Energy-dispersive X-ray spectroscopy (EDS) data of the sample were collected at 20 kV on an ESEM Q250 with a tungsten source equipped with a S10 EDS Bruker AXS detector. Secondary electrons were used to map elemental composition in low vacuum mode. Oxford Instruments AZtec software was used to assign peaks in the EDS spectra. EDS quantification was also performed using the AZtec software package; atomic percentages were determined through peak integration.

2.3.3 UV-vis spectroscopy. A Perkin Elmer Lambda 950 UV-vis-NIR spectrometer was used to measure diffuse reflectance spectra using a 150 mm integrating sphere, in diffuse reflection mode. Spectra were collected from 250–2500 nm, with 2 nm steps. The reference spectrum for total reflectance was measured against a Spectralon disc standard. Samples were suspended in ethanol and drop cast on quartz glass slides (Electron Microscopy Sciences). The slides were dried with nitrogen before measurement. Plots of the Kubelka–Munk function, raised to the power two, *vs.* energy in eV were constructed. Bandgaps were calculated by fitting the linear region in the onset of absorption and extrapolating to the *x*-intercept.

2.3.4 Surface area measurements. The Brunauer–Emmett–Teller (BET) surface area was measured by nitrogen adsorption isotherm measurements (Micromeritics ASAP 2020). The samples were degassed for two hours at 90 °C prior to measurement. A five-point nitrogen adsorption experiment was run and fit by a BET model to obtain the isotherms.

2.3.5 Photoluminescence spectroscopy. The photoluminescence (PL) measurements were performed using a Raman spectrometer (Horiba LabRAM Evolution RAMAN microscope) with 532 nm laser excitation.

2.4 Antimicrobial assays

2.4.1 Bacteria preparation. Three bacterial strains were used in this study, including *S. typhi*, *S. aureus*, and *B. subtilis*. Freshly grown bacterial cells were used for each treatment of photocatalysts. For the preparation of bacterial cells, single colonies were inoculated in tryptic soy broth (TSB) and grew at 37 °C on a shaker for 12 h. The cells were collected in the mid-log phase of the culture with the value of optical density (OD) ~ 0.6 at the wavelength of 595 nm. TSB medium was then removed and the cells were washed twice with phosphate-buffered saline (PBS) by centrifugation (8000 rpm, 5 min). The cells were re-suspended in PBS and diluted with PBS for later treatment. The cell concentration in each treatment was kept at $\sim 5 \times 10^5$ colony-forming units (cfu) per mL.

2.4.2 Antimicrobial test of $CuWO_4$ and CuS. The CuS and $CuWO_4$ suspensions were prepared in deionized (DI) H_2O and sonicated for 10 min before reaction preparations using an ultrasonic water bath (Branson Ultrasonics Corporation, Danbury, CT, USA). The bacteria treatments were performed in 96-well plates. The cells were treated with $CuWO_4$ and CuS alone or in combination with various concentrations in 1/2 PBS, which were prepared using 75 μL of cells in PBS and 75 μL of photocatalysts in DI-H_2O. The plates were placed on a shaker (Lab-Line Instruments, Inc., IL) at the setting of two and exposed to white light (60 W) at a distance of 5 cm for 1 h treatment at room temperature. For comparison, the dark treatment was also included under the same treatment condition as the light treatment, except that the plates were wrapped with aluminum foil to avoid light illumination. A series of 10-fold dilutions of CuS and $CuWO_4$ suspensions were performed immediately after the treatment with the bacterial cells with and without white light irradiation. No attempts were made to try to separate these particles from the cells. A 100 μL aliquot of each dilution was then used to spread on tryptic soy agar (TSA) plates. The viable cell numbers were calculated based on the bacterial colony numbers after 18 h of incubation at 37 °C. Except for the duration of the light treatment, the whole procedure was carried out in the dark. The presence of a highly diluted aqueous suspension of the CuS and $CuWO_4$ particles should have a negligible effect on the final bacterial CFU counts.

2.4.3 Checkerboard assay and fractional inhibitory concentration (FIC) index determination. To study whether there are synergistic antimicrobial interactions between $CuWO_4$ and CuS and to find the most effective $CuWO_4$/CuS combination, a checkerboard method was used, similar to the traditional broth microdilution checkerboard method with some modifications.[24] The experiment was performed in 96-well plates. Aliquots of 50 μL *S. typhi* cells in PBS were added into all the wells. $CuWO_4$ and CuS suspensions with two-fold serial dilutions were prepared in DI-H_2O separately, and then were added into the wells at a volume of 25 μL to achieve two-fold serial dilutions with desired concentrations along the abscissa and ordinate of the plate, respectively, with a final reaction volume of 100 μL in each well. The resulting checkerboard contained all the possible

combinations of the prepared $CuWO_4$ and CuS suspensions, plus $CuWO_4$ and CuS alone. The plates were placed on the shaker and exposed to light for 1 h at room temperature. TSB at a volume of 100 μL was then added into each well. OD_{595} values were measured as growth time 0 using a SpectraMax M5 multidetection reader (Molecular Devices LLC, Sunnyvale, CA, USA) and the plates with the same reactions but without bacterial cells were used as blanks. The plates were incubated at 37 °C in the dark for 18 h, the reactions were homogenized by pipetting up and down for at least 10 times, and OD_{595} values were tested at a growth time of 18 h. The increase in OD_{595} values after growths indicated bacterial growth.

The minimal inhibitory concentration (MIC) of each semiconductor was defined as the lowest concentration that completely inhibited the bacterial growth. The FIC index (∑FIC) was calculated by the use of following equation:

$$\sum FIC = A/MIC_A + B/MIC_B = FIC_A + FIC_B \quad (1)$$

where A and B are the MIC of each hybrid composite (in a single well), and MIC_A and MIC_B are the MIC of individual semiconductor nanocrystals.[29]

The interaction between the two combined reagents was determined by the ∑FIC values as follows: ∑FIC ≤ 0.5 indicates synergy, 0.5 < ∑FIC ≤ 0.75 indicates partial synergy, 0.75 < ∑FIC ≤ 1 indicates additive, 1.0 < ∑FIC < 4.0 indicates indifference, and ∑FIC ≥ 4.0 indicates antagonism.[5,30–32]

2.4.4 Isobologram analysis. To graphically visualize the interactions of $CuWO_4$ and CuS on *S. typhi* bacteria, an isobologram was plotted based on the results of checkerboard assays. In the isobologram, the concentrations of CuS and $CuWO_4$ from the growth–no growth interface were plotted on the *x*- and *y*-axis, respectively, and then the MIC of each nanocrystal alone was plotted and joined by a line on the graph. It was considered as additive interactions if the combination line fell along the line connecting the two MIC values, as synergistic interactions if the combination line fell below, and as antagonistic interactions if the combination line was concave-up.[33,34]

2.4.5 Antimicrobial test of $CuWO_4$/CuS hybrid composites. Hybrid composites of $CuWO_4$/CuS with different weight ratios were used to treat three bacterial strains, including *S. typhi*, *S. aureus*, and *B. subtilis*. The concentrations of $CuWO_4$ and CuS were determined according to the checkerboard results on *S. typhi* and the most effective combination was used together with other combinations for 1 h light treatment. In this way, the most effective combination can be confirmed and optimized. After the treatment, viable cell numbers were tested on TSA plates using the plating methods.

3. Results and discussion

3.1 Characterization of $CuWO_4$ and CuS

3.1.1 Powder XRD analysis. PXRD patterns of as-prepared $CuWO_4$ and as-purchased CuS are shown in Fig. 1. The

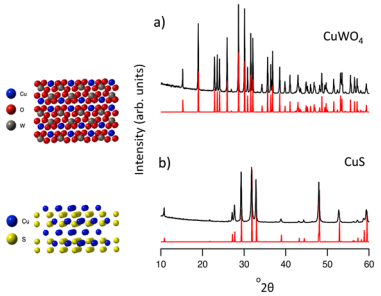

Fig. 1 XRD patterns of a) $CuWO_4$ and b) CuS.

diffraction peaks observed in both samples are identical to simulated patterns for the triclinic phase of $CuWO_4$ (ref. 35) and hexagonal covellite CuS.[36] All peaks matched the reference pattern, and no impurity phases could be observed.

3.1.2 UV-vis diffusive reflectance spectroscopy. The light absorption properties of $CuWO_4$ and CuS were examined using ultraviolet-visible diffuse reflectance spectroscopy. Fig. 2 illustrates the UV-vis diffuse reflectance spectra of $CuWO_4$ and CuS. The optical bandgaps of these two materials were calculated using plots of the Kubelka–Munk function[35–37] *vs.* energy in eV. These materials possess a direct band gap and so the function is raised to the power of two. Bandgaps were calculated by fitting the linear region in the onset of absorption and extrapolating to the *x*-intercept. The calculated band gap values were determined to be 2.4 and 1.8 eV for $CuWO_4$ and CuS, respectively. These values match well with those previously reported in the literature.[38] This indicated that both materials are photosensitive to visible light.

3.1.3 Scanning electron microscopy/energy-dispersive X-ray spectroscopy. The morphologies of these two materials were observed by SEM. SEM images (Fig. 3) reveal that $CuWO_4$ and CuS are polycrystalline with various shapes and that a majority of the crystallites have dimensions ranging from 10 nm to 300 nm. Elemental analysis was performed by energy-dispersive X-ray spectroscopy (EDS) and the spectra of

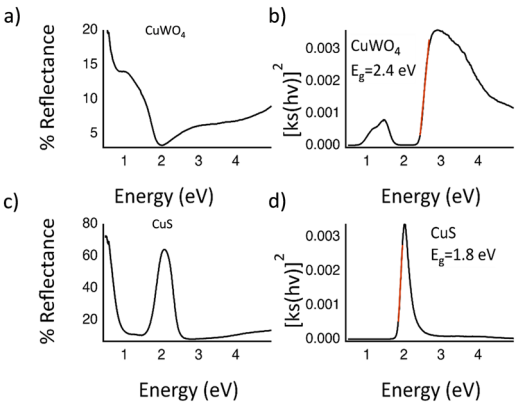

Fig. 2 UV-vis diffuse reflectance spectra of a) $CuWO_4$ and c) CuS, and corresponding direct bandgap calculation: b) $CuWO_4$ and d) CuS utilizing the Kubelka–Munk function.

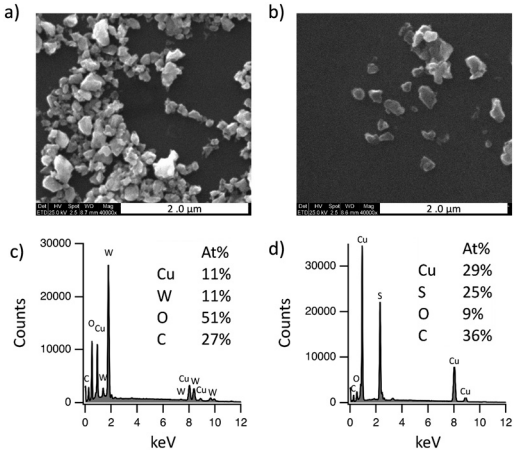

Fig. 3 SEM images of a) $CuWO_4$ and b) CuS, and their corresponding EDS spectra c) and d) for $CuWO_4$ and CuS, respectively. Scale bar: 2.0 μm.

$CuWO_4$ and CuS are shown in Fig. 3c and d, respectively. The EDS spectra confirm the presence of copper (Cu), tungsten (W), and oxygen (O) in $CuWO_4$, and the presence of Cu and sulphur (S) in CuS. All the samples did exhibit a background oxygen and carbon (C) signal from the carbon tape substrate. Subtracting the roughly 10 atomic percent of oxygen signal from the carbon tape, it is found that the Cu : W : O ratio of $CuWO_4$ corresponds to the expected 1 : 1 : 4 ratio. Similarly, CuS exhibits a Cu : S ratio of 1 : 1.

3.2 Antimicrobial assays of pure $CuWO_4$ and CuS

3.2.1 Antimicrobial effects of $CuWO_4$ and CuS. Fig. 4a shows the antimicrobial effects of $CuWO_4$ on *S. typhi* cells after treatment with 8, 16, 32, and 64 μg mL^{-1} $CuWO_4$ for 1 h under visible light illumination or in the dark. With light illumination, $CuWO_4$ showed concentration-dependent antimicrobial effects. When the $CuWO_4$ concentration was 8 μg mL^{-1}, there was a 0.5 log reduction in bacteria population. When the $CuWO_4$ concentration was increased to 64 μg mL^{-1}, there was complete inactivation of the bacteria, with no viable cells detected, a 5.58 log reduction. In contrast, $CuWO_4$ did not show an obvious antimicrobial effect in the dark, even at the concentration of 64 μg mL^{-1}, which confirms that this is a photocatalytic process. This observation was consistent with previous studies, which reported the antimicrobial effects of $CuWO_4$ on bacteria and fungi (*Candida albicans* and *Aspergillus niger*) by disc diffusion methods.[15] As for the antibacterial effect comparison of this study with what was reported by others, there were no prior publications that provided the concentration range of $CuWO_4$ with antimicrobial effects.

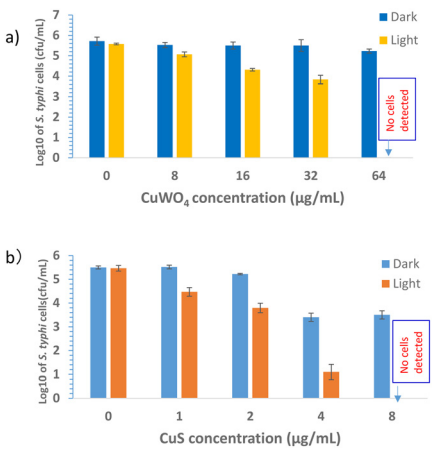

Fig. 4 Antimicrobial effects of $CuWO_4$ (a) and CuS (b) on *S. typhi* cells in the dark or under light. Data is presented as mean values with ± SD error bars.

The antimicrobial activity of $CuWO_4$ depends on several factors, including its degree of agglomeration, molecular weight, nutrient composition, host, natural nutrient constituency, solvent, target microorganism, and physicochemical properties, and is inversely affected by pH.[15,39] Besides the limited application study of $CuWO_4$ on antimicrobial effects, $CuWO_4$ has been utilized to photodegrade hazardous organic and inorganic pollutants, demonstrating excellent activity towards the degradation of ciprofloxacin,[40] MO,[41] MB,[42] tetracycline antibiotic,[43] and terephthalic acid,[44] among other pollutants. Other applications of $CuWO_4$ included photocatalytic water reduction for H_2 generation and photoelectrochemical water splitting.[10]

Fig. 4b shows the antimicrobial effects of individual CuS nanopowders on *S. typhi* cells. Similar to $CuWO_4$, the effects of CuS were light-activated and concentration-dependent. CuS showed obvious antimicrobial effects even at the concentration of 1 μg mL^{-1}, displaying 1 log cell reduction after 1 h light treatment. Meanwhile, CuS at the concentration of 8 μg mL^{-1} completely killed bacteria with 5.5 log reduction. It is worth noting that CuS induces 1.5–2 log cell reduction at high concentrations such as 4 and 8 μg mL^{-1} even without light treatment. The antimicrobial effect of a photocatalyst under dark conditions is called dark toxicity or innate toxicity, which could be attributed to the presence of free metal ions released to the medium. Liang *et al.* found that a certain amount of Cu^{2+} could be released from CuS nanoparticles and Cu^{2+} could damage the structures of DNA, enzymes, and cell membranes, and affect biochemical properties, leading to bacterial death.[19] Giachino and Waldron[45] reported that excess Cu^{2+} is extremely toxic and generated distinctive pleiotropic effects in cells.[20] In our study, it is highly plausible that the Cu^{2+} release from CuS produced excess Cu^{2+} in the environment and caused bacteria death, displaying a cell concentration reduction after treatments in the dark.

Others also reported antimicrobial effects of CuS on bacteria. Liang *et al.*[19] used CuS to treat *S. aureus* infected wounds on the back of rats and observed that CuS had antibacterial properties, and particularly, 500 μg mL^{-1} CuS had good antimicrobial effects without increasing side effects. The authors also indicated that CuS promoted wound healing through re-epithelialization and collagen deposition.[19] Malarkodi and Rajeshkumar[46] synthesized CuS

by using bacteria *Serratia nematodiphila* to reduce $CuSO_4$ into CuS and found that the MIC of CuS against *E. coli*, *S. aureus*, *K. pneumoniae*, and *P. vulgaris* was 30, 40, and 50 μg mL^{-1}, respectively. Huang *et al.*[47] utilized bovine serum albumin (BSA) as the template to synthesize CuS NPs and observed antimicrobial effects on *S. aureus* and *E. coli* cells after being treated with 50 ppm BSA–CuS NPs under near infrared light.

The CuS used in this study was more effective than those used by others[19,42,47] possibly due to the difference in particle size, treatment conditions, bacterium strain, *etc.* It has been demonstrated that CuS nanoparticles interact with the proteins and possible phospholipids associated with the proton pump of bacterial membranes, leading to a collapse of the membrane proton gradient, a disruption of many cellular metabolisms, and cell death.[48,49]

3.3 Interaction of $CuWO_4$ and CuS in combination

Combined treatment of two antimicrobial reagents is generally an effective strategy to inactivate bacteria and also fight resistance.[50] To find the most efficient $CuWO_4$/CuS combination and confirm the synergistic antimicrobial interactions between $CuWO_4$ and CuS, the checkerboard method was used to examine the inhibition of the growth of *S. typhi* cells treated with $CuWO_4$ and CuS separately and in combination. The most efficient combination in this study was considered as the one which could completely kill all the cells with the lowest concentration of $CuWO_4$ and CuS. Fig. 5 illustrates the setup of the checkerboard assay. The MICs of $CuWO_4$ and CuS were 64 and 8 μg mL^{-1}, respectively, showing consistency with the results tested by plating methods above. The FIC indexes were calculated (Table 1). The combination of 8 μg mL^{-1} $CuWO_4$ and 2 μg mL^{-1} CuS showed the $\sum$FIC value of 0.375, which was the lowest $\sum$FIC value among all the combinations, indicating that this combination was the most efficient combination and the interaction between 8 μg mL^{-1} $CuWO_4$ and 2 μg mL^{-1} CuS was synergistic.

The other 2 combinations listed in the table were the combination of 32 μg mL^{-1} $CuWO_4$ with 0.25 μg mL^{-1} CuS, and the combination of 2 μg mL^{-1} $CuWO_4$ with 4 μg mL^{-1} CuS, showing partial synergistic interactions. A different result was observed on the synthesized $CuWO_4$/CuS heterojunction, which showed the best photocatalytic efficacy on the photodegradation of RhB at the ratio of 1 : 1.[28]

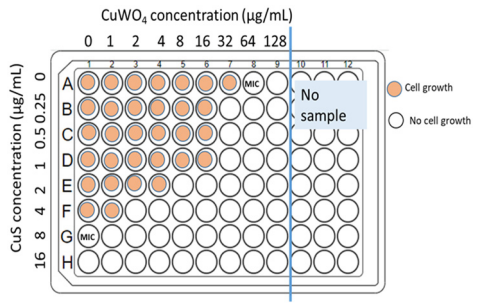

Fig. 5 Illustration of the checkerboard assay results in a 96-well plate using $CuWO_4$ and CuS.

The interaction between $CuWO_4$ and CuS in combination was further tested using isobologram analysis. Isobolograms are an alternative method of interpretation of the interaction of two compounds on a defined microorganism and used when FIC gives borderline values.[33] Fig. 6 shows that the line of MICs in the $CuWO_4$/CuS combination fell below the line of MICs from $CuWO_4$ and CuS treatment alone, indicating the synergistic interaction between $CuWO_4$ and CuS. This observation proved the synergistic relation tested both by the plating method and by the checkerboard method.

Combination treatment of two antimicrobial reagents with synergistic interactions can reduce the frequency of drug resistance and minimize the dosage of toxic drugs, achieving more significant effects than monotherapy in biochemical activity.[51] To achieve a maximal synergistic effect, the determinations of the reagent type, combination ratio, reaction conditions, and screening methods are essential. The checkerboard method developed in this study was easy to handle and could provide sufficient data to find the most efficient combination and to optimize the ratios of two reagents. The major difference between the checkerboard assay in this study and the traditional broth microdilution checkerboard assay[27] was that the cell treatment in this study was performed in 1/2 PBS instead of cell culture medium, and the growth medium was added after the treatment. Our previous study showed that reaction buffers played important roles in the inactivation of bacterial cells and the cell treatment was much more effective in PBS than in broth.[52] As for the most efficient combination in this study, the combination of 8 μg mL^{-1} $CuWO_4$ and 2 μg mL^{-1} CuS reduced 87.5% and 75% dosage of $CuWO_4$ and CuS, respectively, compared to using them separately to reach a complete killing effect. The significant dosage decrease is important on environmental health and reduces economic burden. The synergistic photocatalytic effects were also found in the hybrid composites consisting of $CuWO_4$ with other photocatalysts. For instance, the synergy effects were observed in the combination of $CuWO_4$ and TiO_2 on atrazine degradation, showing an increased degradation efficiency of 92.1% after 270 min, which was 1.94 times higher than that of TiO_2 alone.[53] The spatially separated cocatalysts and p–n heterojunctions in the Pt/$CuWO_4$/Co_3O_4 photoanode system exhibited a prominently enhanced photocurrent of 4.4 mA cm^{-2} at 1.23 V *vs.* RHE, demonstrating that the synergistic effect of this system could effectively achieve improved photoelectrochemical performance for water splitting.[54] The nanostructured ZnO/$CuWO_4$ heterojunction film had a photoelectrochemical degradation efficiency of 82% on RhB, making it approximately twice as effective as ZnO film.[55] It was also observed that the surface modification of $CuWO_4$ with 1.8 wt% CuO can increase the activity by approximately 9 times under UV light and by 5 times under visible light, for phenol degradation in an aerated aqueous suspension.[14]

Table 1 Fractional inhibitory concentration (FIC) index and the interaction between $CuWO_4$ and CuS

$CuWO_4$ concentration (μg mL^{-1})	CuS concentration (μg mL^{-1})	∑FIC	Relation
64	0		MIC of $CuWO_4$
32	0.25	0.53125	Partial synergy
8	2	0.375	Synergy
2	4	0.53125	Partial synergy
0	8	—	MIC of CuS

Abbreviation: MIC, minimal inhibitory concentration.

Although these studies showed the synergistic effects, the authors did not show how to optimize the combination ratios. It is worth noting that the aforementioned photocatalysts such as TiO_2 and ZnO have a bandgap of 3.20 (ref. 9) and 3.37,[44] respectively, which corresponds to an absorption wavelength of 387 and 368 nm, all in the ultraviolet range. The goal of this study was to optimize the synergistic effect of visible light-driven photocatalysts for bacterial inactivation. CuS, with a visible-wavelength bandgap (1.8 eV),[38] is a novel candidate, and such a study using the combination of $CuWO_4$ and CuS has never been reported before.

3.4 Antimicrobial effects of $CuWO_4$/CuS hybrid composites

$CuWO_4$/CuS hybrid composites with varying weight ratios were used to test the effectiveness on *S. typhi*, *S. aureus*, and *B. subtilis*. The concentration of $CuWO_4$ and CuS for the test was determined based on the results from the checkerboard assay. The effect of the mixture consisting of 8 μg mL^{-1} $CuWO_4$ and 2 μg mL^{-1} CuS (denoted as $8CuWO_4$/2CuS) was compared with other combinations through the plating method, including hybrid composites consisting of 8 μg mL^{-1} $CuWO_4$ and 0.5 μg mL^{-1} CuS ($8CuWO_4$/0.5CuS), 8 μg mL^{-1} $CuWO_4$ and 1 μg mL^{-1} CuS ($8CuWO_4$/1CuS), 2 μg mL^{-1} $CuWO_4$ and 2 μg mL^{-1} CuS ($2CuWO_4$/2Cu), and 4 μg mL^{-1} $CuWO_4$ and 2 μg mL^{-1} CuS ($4CuWO_4$/2CuS). The testing results were consistent with the results from the checkerboard assay, showing that the hybrid composite consisting of 8 μg mL^{-1} $CuWO_4$ and 2 μg mL^{-1} CuS was the most effective combination and killed all the tested bacteria, showing ~5.8 log reduction (Fig. 7). This result also proved the reliability of the checkerboard assay.

B. subtilis cells were more vulnerable to the treatments than the other 2 bacterial strains and showed a complete inactivation in all the combinations except for $8CuWO_4$/0.5CuS. By comparing bacteria *S. aureus* and *S. typhi*, the former was more vulnerable to the treatments than the latter in general except for the $4CuWO_4$/2CuS treatment. The possible reason for the difference was that both *B. subtilis* and *S. aureus* are G^+ bacteria, and *S. typhi* is a G^- bacterium. G^+ bacteria usually are more vulnerable to chemical treatments than G^- negative bacteria.[56] Giving an example, in 2017 the World Health Organization (WHO) published a list of antibiotic-resistant priority pathogens, and the majority on the list are G^- bacterial pathogens.[57] The characteristics of G^- bacteria being more resistant to chemicals than G^+ bacteria are due to the cell wall structure difference. The complex G^- bacterial cell wall is made of multiple layers of peptidoglycans, lipoproteins, phospholipids, and lipopolysaccharides, which hampers the penetration of particles in bacterial cells.[56] The outer membrane of G^- bacteria is the main reason for their resistance to a wide range of antibiotics including β-lactams, quinolones, colistins and other antibiotics.[56] The cell wall structure difference might be the explanation for our observation that $CuWO_4$/CuS combinations showed different antimicrobial effects on different bacterial strains.

The XRD patterns of $CuWO_4$/CuS hybrid composites did not show any deleterious phase changes after the photocatalytic bacterial inactivation experiment, as shown in

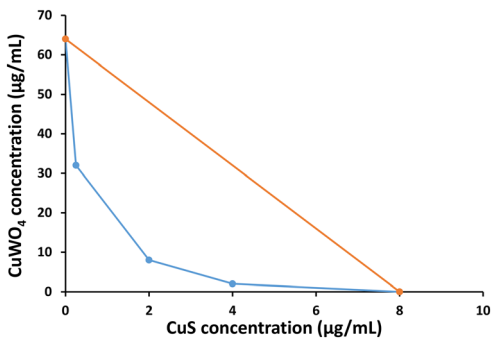

Fig. 6 Isobologram analysis for the $CuWO_4$/CuS combination against *S. typhi* cells.

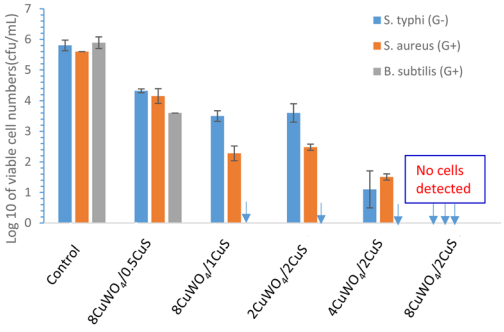

Fig. 7 Antimicrobial effects of $CuWO_4$/CuS combinations. The numbers before the components indicate the concentration (μg mL^{-1}). Data is presented as mean values with ± SD error bars.

Fig. S1, ESI.† The stability of the hybrid composites was also evidenced by EDS mapping and elemental analysis (Fig. S2 and S3, ESI†). The elemental compositions of the hybrid composite only changed slightly after the bacterial inactivation under white light irradiation.

3.5 Proposed mechanisms of photocatalytic inactivation of bacteria

It is generally recognized that after band gap excitation a semiconductor could generate electrons (e^-) and holes (h^+) in its conduction and valence bands, respectively. These charge carriers may recombine to heat or migrate onto the surface, reacting with suitable electron donors and acceptors.[14] Several reactive oxygen species (ROS), such as $^{\bullet}O_2^-$, H_2O_2, $^1O_2$, and $^{\bullet}OH$, are generated through the redox reactions with dissolved oxygen and water.[58] The generation capacity of ROS is the essential factor for photocatalysis. ROS with high oxidative and reductive activities can easily degrade organic and inorganic pollutant molecules.[59] The interaction of ROS with biological microorganisms can cause direct injury to proteins, membrane lipids, and nuclei acids, leading to cell death.[60]

By simply mixing $CuWO_4$ and CuS, synergistic antimicrobial effects were observed in the presence of visible light. The mixture of $CuWO_4$/CuS was similar to the structure of a traditional type-II heterojunction when the two nanopowders were in close contact. The type-II semiconductor heterojunction can be realized when one of the semiconductor's conduction and valence bands is lower than those of its neighboring semiconductor. Thus, the electrons are confined to one material and the holes to the other, preventing electron–hole recombination, manifesting as a quenching of photoluminescence in the heterojunction.[61]

Charge transfer in the $CuWO_4$/CuS composite was probed *via* photoluminescence spectroscopy using a Raman spectrometer. The PL spectra of $CuWO_4$, CuS and the CuS/$CuWO_4$ hybrid composite with a w/w ratio of 1 : 4 are shown in Fig. 8. In the case of the $CuWO_4$/CuS hybrid composite, a strong PL quenching was observed, indicating a charge transfer at the interface of the $CuWO_4$/CuS composite.

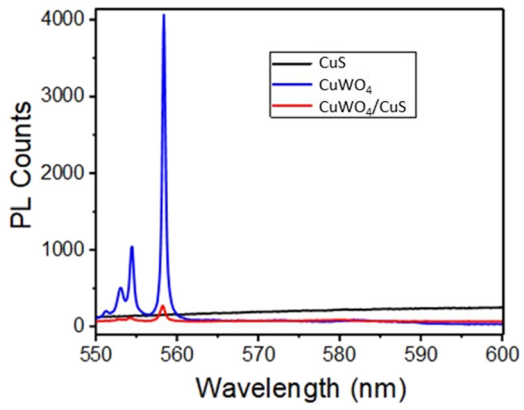

Fig. 8 PL spectra of CuS, $CuWO_4$, and the $CuWO_4$/CuS hybrid composite.

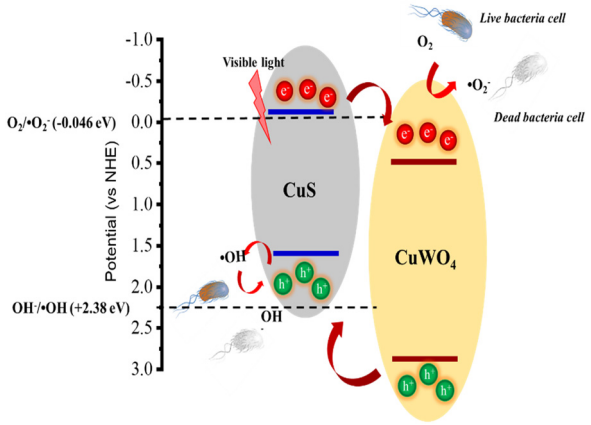

Fig. 9 Proposed mechanism of photocatalytic inactivation of bacteria by the $CuWO_4$/CuS hybrid composite.

The possible mechanisms of photocatalytic inactivation of bacteria are shown in Fig. 9. The E_{cb} and E_{vb} values of $CuWO_4$ and CuS were estimated using the following expressions:[62]

$$E_{vb} = \chi - E_0 + 0.5E_g \quad (2)$$

$$E_{cb} = E_{vb} - E_g \quad (3)$$

where E_{vb} is the valence band (VB) edge potential, the E_0 value is constant 4.5 eV *versus* a normal hydrogen electrode (NHE), E_{cb} is the conduction band (CB) edge potential, E_g is the bandgap of the semiconductor, and χ is the geometric mean of the electronegativities of atoms constituting the semiconductor. The VB position and CB position are estimated to be +2.9 eV and 0.50 eV, respectively for $CuWO_4$,[63,64] whereas these values are +1.67 eV and −0.13 eV respectively for CuS.[65–67]

Under visible light irradiation, $CuWO_4$ and CuS could generate e^- and h^+, and the generated e^- and h^+ could be effectively transferred to the lower potential band. The photo-induced e^- of CuS are transferred to the CB orbitals of $CuWO_4$, and the h^+ of the $CuWO_4$ are transferred to the VB orbitals of CuS. The e^- in the CB orbitals of $CuWO_4$ reduced O_2 to $^{\bullet}O_2^-$, and the h^+ in the VB orbitals of CuS oxidized H_2O to $^{\bullet}OH$ and H_2O_2. The produced ROS reacted with bacteria and caused cell damage, leading to synergistic antimicrobial effects and cell death. A similar mechanism of the degradation of RhB by the $CuWO_4$/CuS heterojunction was reported by Cui *et al.*[28] in which the formation of the $CuWO_4$/CuS heterojunction was evidenced by the significant photoluminescence quenching.

Both $CuWO_4$ and CuS can generate a series of photo-induced reactive species including $^{\bullet}OH$ and $^{\bullet}O_2^-$ with the irradiation of visible light.[68,69] $CuWO_4$ and CuS have been reported for their capabilities to effectively degrade various pollutants.[68,69] The ROS generation by $CuWO_4$ could be the

explanation for the antimicrobial effects in this study. The difference in band gap also allows them to function synergistically under illumination. This supports our hypothesis that interfacing these two materials could lead to superior separation and stabilization of photogenerated e^- and h^+. Charge transfer is energetically favorable because of the misalignment of the valance and condition band edges.

Although individual semiconductor photocatalysts might show good photocatalytic efficiencies when the reaction conditions are suitable, using a single photocatalyst may face a drawback since photoproduced e^- and h^+ pairs are generally likely to recombine, leading to reduced quantum and photocatalytic efficiencies.[70,71] However, this drawback can be improved by coupling with another photocatalyst which can effectively increase the separation of e^- and h^+. The heterojunction photocatalysts typically could be grouped into six categories based on the heterojunction structure: traditional (*e.g.*, type I, type II, and type III), p–n, Z-scheme, step-scheme, Schottky, and surface heterojunctions.[59,72,73] In terms of traditional heterojunction systems, only the type II heterojunction can be an ideal system to improve the separation of e^- and h^+. In type II heterojunctions, the e^- transfers to the semiconductor with a lower CB level. Meanwhile, the h^+ transfers to the semiconductor with a higher VB level, decreasing the contact and recombination of electron–hole pairs.[59,74]

The photocatalytic efficiency of the photo-induced degradation varies over a wide range due to the type of photocatalyst used and the solution conditions employed.[54] A narrow bandgap, large specific surface area and efficiency of the separation of photoexcited electrons and holes were the essential factors for the enhanced photocatalytic activity.[28] N_2 adsorption isotherms were obtained for a) CuS, b) $CuWO_4$, and c) the CuS/$CuWO_4$ hybrid composite with a w/w ratio of 1 : 4 (see Fig. S4 – ESI†). The BET surface areas of CuS, $CuWO_4$, and the CuS/$CuWO_4$ hybrid composite were determined to be 0.5, 1.4, and 8.0 $m^2\ g^{-1}$, respectively, confirming an increase of the surface area as a result of ultrasound-assisted physical mixing.

4. Conclusions

In this study, a checkerboard method was developed by the modification of the traditional broth microdilution checkerboard assay to examine the antibacterial efficacy of $CuWO_4$ and CuS nanopowders individually and in mixtures of varying weight ratios. This method provided a way to find the best and most effective combination of antimicrobial photocatalysts. The hybrid composite consisting of 8 μg mL^{-1} $CuWO_4$ and 2 μg mL^{-1} CuS was found to generate the maximum synergistic effect, showing a complete killing effect on all three bacteria with ~5.8 log cell reduction. The potent antimicrobial effects of $CuWO_4$/CuS hybrid composites made it a feasible strategy to inactivate pathogenic bacteria in the environment in a fast (in 1 h), easy, and effective manner. These findings have significant implications for the coupling of semiconductors with suitable bandgaps to develop new and effective antimicrobial materials for water disinfection.

Author contributions

XD and FY designed this study. XD, RK, and LH performed the laboratory experiments. XD and RK evaluated the data and drafted the manuscript. BC, LY, RS, and FY revised the manuscript. All the authors accepted to submit for publication.

Conflicts of interest

There are no conflicts to declare.

Acknowledgements

XD, BC, and FY are grateful for the financial support of this project by the U.S. National Science Foundation (Awards #1831133 and #2122044). This material is based upon work supported in part by the U. S. Army Research Office under contract number W911NF2210109. RK and RS thank Penn State University for funding. LH acknowledges RTI International for funding support.

References

1 E. Scallan, R. M. Hoekstra, F. J. Angulo, R. V. Tauxe, M. A. Widdowson, S. L. Roy, J. L. Jones and P. M. Griffin, Foodborne illness acquired in the United States–major pathogens, *Emerging Infect. Dis.*, 2011, **17**, 7–15.

2 J. H. Nakao, D. Talkington, C. A. Bopp, J. Besser, M. L. Sanchez, J. Guarisco, S. L. Davidson, C. Warner, M. G. McIntyre, J. P. Group, N. Comstock, K. Xavier, T. S. Pinsent, J. Brown, J. M. Douglas, G. A. Gomez, N. M. Garrett, H. A. Carleton, B. Tolar and M. E. Wise, Unusually high illness severity and short incubation periods in two foodborne outbreaks of *Salmonella Heidelberg* infections with potential coincident *Staphylococcus aureus* intoxication, *Epidemiol. Infect.*, 2018, **146**, 19–27.

3 P. R. McAdam, K. E. Templeton, G. F. Edwards, M. T. G. Holden, E. J. Feil, D. M. Aanensen, H. J. A. Bargawi, B. G. Spratt, S. D. Bentley, J. Parkhill, M. C. Enright, A. Holmes, E. K. Girvan, P. A. Godfrey, M. Feldgarden, A. M. Kearns, A. Rambaut, D. A. Robinson and J. R. Fitzgerald, Molecular tracing of the emergence, adaptation, and transmission of hospital-associated methicillin-resistant *Staphylococcus aureus*, *Proc. Natl. Acad. Sci. U. S. A.*, 2012, **109**, 9107–9112.

4 A. K. Goel, Anthrax: A disease of biowarfare and public health importance, *World J. Clin. Cases*, 2015, **3**, 20–33.

5 X. L. Dong, M. Al Awak, N. Tomlinson, Y. G. Tang, Y. P. Sun and L. J. Yang, Antibacterial effects of carbon dots in combination with other antimicrobial reagents, *PLoS One*, 2017, **12**, e0185324.

6 N. Ding, X. M. Chang, N. Shi, X. F. Yin, F. Qi and Y. X. Sun, Enhanced inactivation of antibiotic-resistant bacteria isolated from secondary effluents by g-C_3N_4 photocatalysis, *Environ. Sci. Pollut. Res.*, 2019, **26**, 18730–18738.

7 P. Lozovskis, V. Jankauskaite, A. Guobiene, V. Kareiviene and A. Vitkauskiene, Effect of graphene oxide and silver nanoparticles hybrid composite on *P. aeruginosa* strains with acquired resistance genes, *Int. J. Nanomed.*, 2020, **15**, 5147–5163.
8 T. Matsunaga, R. Tomoda, T. Nakajima and H. Wake, Photoelectrochemical sterilization of microbial cells by semiconductor powders, *FEMS Microbiol. Lett.*, 1985, **29**, 211–214.
9 P. Wang, B. Huang, X. Qin, X. Zhang, Y. Dai and M. H. Whangbo, Ag/AgBr/WO(3).H(2)O: visible-light photocatalyst for bacteria destruction, *Inorg. Chem.*, 2009, **48**, 10697–10702.
10 P. Raizada, S. Sharma, A. Kumar, P. Singh, A. A. P. Khan and A. M. Asiri, Performance improvement strategies of $CuWO_4$ photocatalyst for hydrogen generation and pollutant degradation, *J. Environ. Chem. Eng.*, 2020, **8**, 104230.
11 F. A. Benko, C. L. Maclaurin and F. P. Koffyberg, $CuWO_4$ and Cu_3WO_6 as anodes for the photoelectrolysis of Water, *Mater. Res. Bull.*, 1982, **17**, 133–136.
12 J. E. Yourey, K. J. Pyper, J. B. Kurtz and B. M. Bartlett, Chemical stability of $CuWO_4$ for photoelectrochemical water oxidation, *J. Phys. Chem. C*, 2013, **117**, 8708–8718.
13 J. C. Hill and K. S. Choi, Synthesis and characterization of high surface area $CuWO_4$ and Bi_2WO_6 electrodes for use as photoanodes for solar water oxidation, *J. Mater. Chem. A*, 2013, **1**, 5006–5014.
14 H. H. Chen, W. H. Leng and Y. M. Xu, Enhanced visible-light photoactivity of $CuWO_4$ through a surface-deposited CuO, *J. Phys. Chem. C*, 2014, **118**, 9982–9989.
15 B. Kavitha and R. Karthiga, Synthesis and characterization of $CuWO_4$ as nano-adsorbent for removal of Nile blue and its antimicrobial studies, *J. Mater. Environ. Sci.*, 2020, **11**, 57–68.
16 R. Gupta, B. Boruah, J. M. Modak and G. Madras, Kinetic study of Z-scheme $C_3N_4/CuWO_4$ photocatalyst towards solar light inactivation of mixed populated bacteria, *J. Photochem. Photobiol., A*, 2019, **372**, 108–121.
17 K. Vignesh, R. Priyanka, R. Hariharan, M. Rajarajan and A. Suganthi, Fabrication of CdS and $CuWO_4$ modified TiO_2 nanoparticles and its photocatalytic activity under visible light irradiation, *J. Ind. Eng. Chem.*, 2014, **20**, 435–443.
18 W. C. Xu, S. L. Zhu, Y. Q. Liang, Z. Y. Li, Z. D. Cui, X. J. Yang and A. Inoue, Nanoporous CuS with excellent photocatalytic property, *Sci. Rep.*, 2015, **5**, 18125.
19 Y. Liang, J. L. Zhang, H. H. Quan, P. Zhang, K. T. Xu, J. S. He, Y. C. Fang, J. C. Wang and P. T. Chen, Antibacterial effect of copper sulfide nanoparticles on infected wound healing, *Surg. Infect.*, 2021, **22**, 894–902.
20 E. Addae, X. L. Dong, E. McCoy, C. Yang, W. Chen and L. J. Yang, Investigation of antimicrobial activity of photothermal therapeutic gold/copper sulfide core/shell nanoparticles to bacterial spores and cells, *J. Biol. Eng.*, 2014, **8**, 11.
21 A. Swaidan, S. Ghayyem, A. Barras, A. Addad, S. Szunerits and R. Boukherroub, Enhanced antibacterial activity of CuS-BSA/lysozyme under near infrared light irradiation, *Nanomaterials*, 2021, **11**, 2156.
22 T. P. Mofokeng, M. J. Moloto, P. M. Shumbula, P. Nyamukamba, P. K. Mubiayi, S. Takaidza and L. Marais, Antimicrobial activity of amino acid-capped zinc and copper sulphide nanoparticles, *J. Nanotechnol.*, 2018, **2018**, 4902675.
23 P. Raizada, A. Sudhaik, P. Singh, A. Hosseini-Bandegharaei and P. Thakur, Converting type II AgBr/VO into ternary Z scheme photocatalyst via coupling with phosphorus doped g-C_3N_4 for enhanced photocatalytic activity, *Sep. Purif. Technol.*, 2019, **227**, 115692.
24 J. Luo, P. Lin, P. Zheng, X. Zhou, X. Ning, L. Zhan, Z. Wu, X. Liu and X. Zhou, In suit constructing S-scheme FeOOH/MgIn2S4 heterojunction with boosted interfacial charge separation and redox activity for efficiently eliminating antibiotic pollutant, *Chemosphere*, 2022, **298**, 134297.
25 J. Luo, X. Zhou, F. Yang, X. Ning, L. Zhan, Z. Wu and X. Zhou, Generating a captivating S-scheme CuBi2O4/CoV2O6 heterojunction with boosted charge spatial separation for efficiently removing tetracycline antibiotic from wastewater, *J. Cleaner Prod.*, 2022, **357**, 131992.
26 J. Luo, J. Chen, X. Chen, X. Ning, L. Zhan and X. Zhou, Construction of cerium oxide nanoparticles immobilized on the surface of zinc vanadate nanoflowers for accelerated photocatalytic degradation of tetracycline under visible light irradiation, *J. Colloid Interface Sci.*, 2021, **587**, 831–844.
27 J. A. Moody, in *Clinical microbiology procedures handbook*, ed. H. D. Eisenberg, American Society for Microbiology, Washington, DC, 1992, pp. 5.18.11–15.18.23.
28 Y. Y. Cui, C. C. Lin, M. K. Li, N. L. Zhu, J. J. Meng and J. T. Zhao, $CuWO_4$/CuS heterojunction photocatalyst for the application of visible-light-driven photodegradation of dye pollutions, *J. Alloys Compd.*, 2022, **893**, 162181.
29 S. K. Pillai, R. C. Moellering Jr. and G. M. Eliopoulos, in *Antibiotics In Laboratory Medicine*, ed. V. Lorian, Lippincott Williams & Wilkins, Philadelphia, PA, 5th edn, 2005, ch. 9, pp. 365–441.
30 Y. Cai, R. Wang, F. Pei and B. B. Liang, Antibacterial activity of allicin alone and in combination with beta-lactams against *Staphylococcus* spp. and *Pseudomonas aeruginosa*, *J. Antibiot.*, 2007, **60**, 335–338.
31 X. L. Dong, A. E. Bond, N. Y. Pan, M. Coleman, Y. G. Tang, Y. P. Sun and L. J. Yang, Synergistic photoactivated antimicrobial effects of carbon dots combined with dye photosensitizers, *Int. J. Nanomed.*, 2018, **13**, 8025–8035.
32 G. Roks, C. L. P. Deckers, H. Meinardi, R. Dirksen, J. Van Egmond and C. M. van Rijn, Effects of polytherapy compared with monotherapy in antiepileptic drugs: An animal study, *J. Pharmacol. Exp. Ther.*, 1999, **288**, 472–477.
33 M. Badaoui Najjar, D. Kashtanov and M. L. Chikindas, Epsilon-poly-L-lysine and nisin A act synergistically against Gram-positive food-borne pathogens *Bacillus cereus* and *Listeria monocytogenes*, *Lett. Appl. Microbiol.*, 2007, **45**, 13–18.
34 K. S. Kaushik, J. Stolhandske, O. Shindell, H. D. Smyth and V. D. Gordon, Tobramycin and bicarbonate synergise to kill planktonic *Pseudomonas aeruginosa*, but antagonise to promote biofilm survival, *npj Biofilms Microbiomes*, 2016, **2**, 16006.

35 H. Fjellvag, F. Gronvold, S. Stolen, A. F. Andresen, R. Mullerkafer and A. Simon, Low-temperature structural distortion in Cus, *Z. Kristallogr.*, 1988, **184**, 111–121.

36 D. J. Jovanovic, I. L. Validzic, M. Mitric and J. M. Nedeljkovic, Synthesis and structural characterization of nano-sized copper tungstate particles, *Acta Chim. Slov.*, 2012, **59**, 70–74.

37 A. Escobedo-Morales, I. I. Ruiz-Lopez, M. D. Ruiz-Peralta, L. Tepech-Carrillo, M. Sanchez-Cantu and J. E. Moreno-Orea, Automated method for the determination of the band gap energy of pure and mixed powder samples using diffuse reflectance spectroscopy, *Heliyon*, 2019, **5**, e01505.

38 A. E. B. Lima, M. J. S. Costa, R. S. Santos, N. C. Batista, L. S. Cavalcante, E. Longo and G. E. Luz, Facile preparation of $CuWO_4$ porous films and their photoelectrochemical properties, *Electrochim. Acta*, 2017, **256**, 139–145.

39 S. Gunalan, R. Sivaraj and V. Rajendran, Green synthesized ZnO nanoparticles against bacterial and fungal pathogens, *Prog. Nat. Sci.: Mater. Int.*, 2012, **22**, 695–702.

40 M. Thiruppathi, J. V. Kumar, M. Vahini, C. Ramalingan and E. R. Nagarajan, A study on divergent functional properties of sphere-like $CuWO_4$ anchored on 2D graphene oxide sheets towards the photocatalysis of ciprofloxacin and electrocatalysis of methanol, *J. Mater. Sci.: Mater. Electron.*, 2019, **30**, 10172–10182.

41 F. Ahmadi, M. Rahimi-Nasrabadi and M. Eghbali-Arani, The synthesize of $CuWO_4$ nano particles by a new morphological control method, characterization of its photocatalytic activity, *J. Mater. Sci.: Mater. Electron.*, 2017, **28**, 5244–5249.

42 A. Rashidizadeh, H. Ghafuri and Z. Rezazadeh, Improved visible-light photocatalytic activity of g-C_3N_4/$CuWO_4$ nanocomposite for degradation of methylene blue, *Proceedings*, 2020, **41**, 43.

43 W. C. Ding, X. N. Wu and Q. F. Lu, Structure and photocatalytic activity of thin-walled $CuWO_4$ nanotubes: An experimental and DFT study, *Mater. Lett.*, 2019, **253**, 323–326.

44 T. Mavric, M. Valant, M. Forster, A. J. Cowan, U. Lavrencic and S. Emin, Design of a highly photocatalytically active ZnO/$CuWO_4$ nanocomposite, *J. Colloid Interface Sci.*, 2016, **483**, 93–101.

45 A. Giachino and K. J. Waldron, Copper tolerance in bacteria requires the activation of multiple accessory pathways, *Mol. Microbiol.*, 2020, **114**, 377–390.

46 C. Malarkodi and S. Rajeshkumar, In vitro bactericidal activity of biosynthesized CuS nanoparticles against UTI-causing pathogens, *Inorg. Nano-Met. Chem.*, 2017, **47**, 1290–1297.

47 J. Huang, J. Zhou, J. Zhuang, H. Gao, D. Huang, L. Wang, W. Wu, Q. Li, D. P. Yang and M. Y. Han, Strong Near-Infrared Absorbing and Biocompatible CuS nanoparticles for rapid and efficient photothermal ablation of Gram-positive and -negative bacteria, *ACS Appl. Mater. Interfaces*, 2017, **9**, 36606–36614.

48 D. Ayodhya and G. Veerabhadram, Preparation, characterization, photocatalytic, sensing and antimicrobial studies of *Calotropis gigantea* leaf extract capped CuS NPs by a green approach, *J. Inorg. Organomet. Polym. Mater.*, 2017, **27**, S215–S230.

49 P. Dibrov, J. Dzioba, K. K. Gosink and C. C. Hase, Chemiosmotic mechanism of antimicrobial activity of Ag+ in *Vibrio cholerae*, *Antimicrob. Agents Chemother.*, 2002, **46**, 2668–2670.

50 X. J. Xu, L. Xu, G. J. Yuan, Y. M. Wang, Y. Q. Qu and M. J. Zhou, Synergistic combination of two antimicrobial agents closing each other's mutant selection windows to prevent antimicrobial resistance, *Sci. Rep.*, 2018, **8**, 7237.

51 J. B. Fitzgerald, B. Schoeberl, U. B. Nielsen and P. K. Sorger, Systems biology and combination therapy in the quest for clinical efficacy, *Nat. Chem. Biol.*, 2006, **2**, 458–466.

52 X. L. Dong, M. Al Awak, P. Wang, Y. P. Sun and L. J. Yang, Carbon dot incorporated multi-walled carbon nanotube coated filters for bacterial removal and inactivation, *RSC Adv.*, 2018, **8**, 8292–8301.

53 D. W. He, Y. Yang, J. J. Tang, K. G. Zhou, W. Chen, Y. Q. Chen and Z. J. Dong, Synergistic effect of TiO_2-$CuWO_4$ on the photocatalytic degradation of atrazine, *Environ. Sci. Pollut. Res.*, 2019, **26**, 12359–12367.

54 Z. F. Liu, Q. G. Song, M. Zhou, Z. G. Guo, J. H. Kang and H. Y. Yan, Synergistic enhancement of charge management and surface reaction kinetics by spatially separated cocatalysts and p-n heterojunctions in Pt/$CuWO_4$/Co_3O_4 photoanode, *Chem. Eng. J.*, 2019, **374**, 554–563.

55 J. P. C. Moura, R. Y. N. Reis, A. E. B. Lima, R. S. Santos and G. E. Luz, Improved photoelectrocatalytic properties of ZnO/$CuWO_4$ heterojunction film for RhB degradation, *J. Photochem. Photobiol., A*, 2020, **401**, 112778.

56 Z. Breijyeh, B. Jubeh and R. Karaman, Resistance of Gram-negative bacteria to current antibacterial agents and approaches to resolve It, *Molecules*, 2020, **25**, 1340.

57 G. V. Asokan, T. Ramadhan, E. Ahmed and H. Sanad, WHO global priority pathogens list: a bibliometric analysis of Medline-PubMed for knowledge mobilization to infection prevention and control practices in Bahrain, *Oman Med. J.*, 2019, **34**, 184–193.

58 Y. Nosaka and A. Y. Nosaka, Generation and detection of reactive oxygen species in photocatalysis, *Chem. Rev.*, 2017, **117**, 11302–11336.

59 X. H. He, T. H. Kai and P. Ding, Heterojunction photocatalysts for degradation of the tetracycline antibiotic: a review, *Environ. Chem. Lett.*, 2021, **19**, 4563–4601.

60 I. S. Arts, A. Gennaris and J. F. Collet, Reducing systems protecting the bacterial cell envelope from oxidative damage, *FEBS Lett.*, 2015, **589**, 1559–1568.

61 X. Hong, J. Kim, S.-F. Shi, Y. Zhang, C. Jin, Y. Sun, S. Tongay, J. Wu, Y. Zhang and F. Wang, Ultrafast charge transfer in atomically thin MoS_2/WS_2 heterostructures, *Nat. Nanotechnol.*, 2014, **9**, 682–686.

62 N. Jatav, J. Kuntail, D. Khan, A. Kumar De and I. Sinha, AgI/$CuWO_4$ Z-scheme photocatalyst for the degradation of organic pollutants: Experimental and molecular dynamics studies, *J. Colloid Interface Sci.*, 2021, **599**, 717–729.

63 K. Li, C. Zhang, X. Li, Y. Du, P. Yang and M. Zhu, A nanostructured $CuWO_4/Mn_3O_4$ with p/n heterojunction as photoanode toward enhanced water oxidation, *Catal. Today*, 2019, **335**, 173–179.

64 A. E. B. Lima, M. Assis, A. L. S. Resende, H. L. S. Santos, L. H. Mascaro, E. Longo, R. S. Santos, L. S. Cavalcante and G. E. Luz, $CuWO_4|MnWO_4$ heterojunction thin film with improved photoelectrochemical and photocatalytic properties using simulated solar irradiation, *J. Solid State Electrochem.*, 2022, **26**, 997–1011.

65 A. Prakash, M. Dan, S. Yu, S. Wei, Y. Li, F. Wang and Y. Zhou, In_2S_3/CuS nanosheet composite: An excellent visible light photocatalyst for H_2 production from H_2S, *Sol. Energy Mater. Sol. Cells*, 2018, **180**, 205–212.

66 L. Guo, K. Zhang, X. Han, Q. Zhao, D. Wang and F. Fu, 2D In-plane CuS/Bi_2WO_6 p-n heterostructures with promoted visible-light-driven photo-fenton degradation performance, *Nanomaterials*, 2019, **9**, 1151.

67 Q. Chen, M. Zhang, J. Li, G. Zhang, Y. Xin and C. Chai, Construction of immobilized 0D/1D heterostructure photocatalyst $Au/CuS/CdS/TiO_2$ NBs with enhanced photocatalytic activity towards moxifloxacin degradation, *Chem. Eng. J.*, 2020, **389**, 124476.

68 L. M. Liang, H. Liu, Y. Tian, Q. Y. Hao, C. C. Liu, W. C. Wang and X. J. Xie, Fabrication of novel $CuWO_4$ hollow microsphere photocatalyst for dye degradation under visible-light irradiation, *Mater. Lett.*, 2016, **182**, 302–304.

69 S. Adhikari, D. Sarkar and G. Madras, Hierarchical design of CuS architectures for visible light photocatalysis of 4-chlorophenol, *ACS Omega*, 2017, **2**, 4009–4021.

70 B. Louangsouphom, X. J. Wang, J. K. Song and X. Wang, Low-temperature preparation of a N-TiO_2/macroporous resin photocatalyst to degrade organic pollutants, *Environ. Chem. Lett.*, 2019, **17**, 1061–1066.

71 T. Soltani, A. Tayyebi and B. K. Lee, Photolysis and photocatalysis of tetracycline by sonochemically heterojunctioned $BiVO_4$/reduced graphene oxide under visible-light irradiation, *J. Environ. Manage.*, 2019, **232**, 713–721.

72 X. H. He, A. Z. Wang, P. Wu, S. B. Tang, Y. Zhang, L. Li and P. Ding, Photocatalytic degradation of microcystin-LR by modified TiO_2 photocatalysis: A review, *Sci. Total Environ.*, 2020, **743**, 140694.

73 X. R. Yang, Z. Chen, W. Zhao, C. X. Liu, X. X. Qian, M. Zhang, G. Y. Wei, E. Khan, Y. H. Ng and Y. S. Ok, Recent advances in photodegradation of antibiotic residues in water, *Chem. Eng. J.*, 2021, **405**, 126806.

74 H. L. Zhou, Y. Q. Qu, T. Zeid and X. F. Duan, Towards highly efficient photocatalysts using semiconductor nanoarchitectures, *Energy Environ. Sci.*, 2012, **5**, 6732–6743.

